



Dimethyloxallylglycine Prevents Bone Loss in Ovariectomized C57BL/6J Mice through Enhanced Angiogenesis and Osteogenesis

Jia Peng¹*, Zuo Gui Lai^{1,2}*, Zhang Lian Fang^{1,3}, Shen Xing¹, Kang Hui¹, Chen Hao¹, Qi Jin¹, Zhou Qi¹, Wang Jin Shen¹, Qian Nian Dong¹, Zhou Han Bing¹, Deng Lian Fu^{1*}

1 Shanghai Institute of Traumatology and Orthopaedics, Shanghai Key Laboratory for Prevention and Treatment of Bone and Joint Diseases with Integrated Chinese-Western Medicine, Ruijin Hospital, Jiao Tong University School of Medicine, Shanghai, China, **2** Department of Orthopaedics, Qian Fo Shan Hospital, Shang Dong University, Ji Nan, China, **3** Department of Orthopaedics, The First Affiliated Hospital of Soochow University, Suzhou, China

Abstract

Hypoxia-inducible factor 1- α (HIF-1 α) plays a critical role in angiogenesis-osteogenesis coupling during bone development and bone regeneration. Previous studies have shown that 17 β -estradiol activates the HIF-1 α signaling pathway and that mice with conditional activation of the HIF-1 α signaling pathway in osteoblasts are protected from ovariectomy (OVX)-induced bone loss. In addition, it has been shown that hypoxia facilitates the osteogenic differentiation of mesenchymal stem cells (MSCs) and modulates Wnt/ β -catenin signaling. Therefore, we hypothesized that activation of the HIF-1 α signaling pathway by hypoxia-mimicking agents would prevent bone loss due to estrogen deficiency. In this study, we confirmed the effect of dimethyloxallylglycine (DMOG), a hypoxia-mimicking agent, on the HIF-1 α signaling pathway and investigated the effect of DMOG on MSC osteogenic differentiation and the Wnt/ β -catenin signaling pathway. We then investigated the effect of DMOG treatment on OVX-induced bone loss. Female C57BL/6J mice were divided into sham, OVX, OVX+L-DMOG (5 mg/kg/day), and OVX+H-DMOG (20 mg/kg/day) groups. At sacrifice, static and dynamic bone histomorphometry were performed with micro computed tomography (micro-CT) and undecalcified sections, respectively. Bone strength was assessed with the three-point bending test, and femur vessels were reconstructed and analyzed by micro-CT. Serum vascular endothelial growth factor (VEGF), osteocalcin, and C-terminal telopeptides of collagen type (CTX) were measured by ELISA. Tartrate-resistant acid phosphatase staining was used to assess osteoclast formation. Alterations in the HIF-1 α and Wnt/ β -catenin signaling pathways in the bone were detected by western blot. Our results showed that DMOG activated the HIF-1 α signaling pathway, which further activated the Wnt/ β -catenin signaling pathway and enhanced MSC osteogenic differentiation. The micro-CT results showed that DMOG treatment improved trabecular bone density and restored the bone microarchitecture and blood vessels in OVX mice. Bone strength was also partly restored in DMOG-treated OVX mice. Dynamic bone histomorphometric analysis of the femur metaphysis revealed that DMOG increased the mineralizing surface, mineral apposition rate, and bone formation rate. The serum levels of VEGF and osteocalcin were higher in DMOG-treated OVX mice. However, there were no significant differences in serum CTX or in the number of tartrate-resistant acid phosphatase-stained cells between DMOG-treated OVX mice and OVX mice. Western blot results showed that DMOG administration partly rescued the decrease in HIF-1 α and β -catenin expression following ovariectomy. Collectively, these results indicate that DMOG prevents bone loss due to ovariectomy in C57BL/6J mice by enhancing angiogenesis and osteogenesis, which are associated with activated HIF-1 α and Wnt/ β -catenin signaling pathways.

Citation: Peng J, Lai ZG, Fang ZL, Xing S, Hui K, et al. (2014) Dimethyloxallylglycine Prevents Bone Loss in Ovariectomized C57BL/6J Mice through Enhanced Angiogenesis and Osteogenesis. PLoS ONE 9(11): e112744. doi:10.1371/journal.pone.0112744

Editor: Rajeev Samant, University of Alabama at Birmingham, United States of America

Received: July 17, 2014; **Accepted:** October 12, 2014; **Published:** November 13, 2014

Copyright: © 2014 Peng et al. This is an open-access article distributed under the terms of the Creative Commons Attribution License, which permits unrestricted use, distribution, and reproduction in any medium, provided the original author and source are credited.

Data Availability: The authors confirm that all data underlying the findings are fully available without restriction. All relevant data are available within Supporting Information files.

Funding: Deng Lian Fu received funds from Natural Science Foundation of China (No. 81371958, 81061160510), the Basic Key Project of Science and Technology Commission of Shanghai Municipality (12JC1408200), and the Scientific and Technological Support Program in Biological Medicine of Science and Technology Commission of Shanghai Municipality (13431900702) <http://www.nsf.gov.cn/> <http://www.stcsm.gov.cn/>. The funders had no role in study design, data collection and analysis, decision to publish, or preparation of the manuscript.

Competing Interests: The authors have declared that no competing interests exist.

* Email: china_boneres@163.com

† These authors contributed equally to this work.

Introduction

Osteoporosis is a disorder characterized by increased bone fragility, low bone mass, and a consequent increase in fracture risk [1]. Fragility fractures resulting from osteoporosis are the main cause of disablement and death among elderly women. These

events lead to the consumption of enormous amounts of medical resources and produce heavy economic burdens [2]. Therefore, using current understanding of disease pathogenesis to develop effective drugs for the prevention and treatment of postmenopausal osteoporosis is vital.

The skeleton is a highly vascularized tissue in which bone remodeling is tightly coupled with angiogenesis. The vasculature supplies nutrients, oxygen, and mesenchymal stem cells (MSCs), which are necessary elements for bone formation, and may direct new bone formation by providing a scaffold for bone-forming cells [3]. Although the main cause of postmenopausal osteoporosis is estrogen deficiency, accumulating evidence from studies in cells, animals, and patients suggests that the local blood supply or decreased angiogenesis contributes to estrogen deficiency-induced osteoporosis [4–11].

Angiogenesis depends on hypoxic stimuli and vascular endothelial growth factor (VEGF) production. The hypoxia-inducible factor- α (HIF- α) pathway is the central regulator of the adaptive response to low oxygen levels. The pathway regulates angiogenic genes (e.g., *VEGF*, *angiopoietins*). The HIF family comprises three α subunits, HIF-1 α , HIF-2 α , and HIF-3 α . HIF- α is an oxygen-labile protein that forms a heterodimeric complex with the HIF- β subunit, which is constitutively expressed [12]. Under normoxic conditions, HIF- α is hydroxylated at a proline residue by prolyl hydroxylases (PHDs), which need oxygen, iron, and 2-oxyglutarate as cofactors. When hydroxylated, HIF- α is bound by von Hippel-Lindau protein (pVHL), an E3 ubiquitin ligase, and is then degraded by the proteasome. Under hypoxic conditions, prolyl hydroxylation of HIF- α is inhibited, and HIF- α accumulates in the nucleus, where it heterodimerizes with the HIF- β subunit and transactivates HIF responsive genes [13–15]. The HIF pathway can be activated under normoxic conditions by small molecule inhibitors of PHDs that interfere with the required PHD cofactors by acting as iron chelators (e.g., desferrioxamine (DFO)) or 2-oxyglutarate analogues (e.g., dimethylxalylglycine (DMOG)) [14,16].

Importantly, the HIF- α pathway plays a critical role in angiogenesis-osteogenesis coupling. Clemens *et al.* showed that activation of the HIF- α pathway in mature osteoblasts in developing bone increased bone modeling and the effect was largely attributed to enhanced VEGF-mediated bone vessel formation [17]. Similar results were reported by Giaccia *et al.*, who generated mice in which HIF- α was overstabilized in osteoprogenitor cells. The mice exhibited excessive accumulation of trabecular bone in the long bone and increased vascularization [18]. Striking and progressive accumulation of cancellous bone with increased microvascular density and bone formation was also observed in mice lacking *Vhl* in osteochondral progenitor cells [19]. Moreover, the HIF-1 α pathway was activated during bone repair and could be manipulated genetically and pharmacologically to accelerate bone regeneration [16,20]. Consistent with the “promoting osteogenesis by enhancing angiogenesis” theory, HIF-1 α pathway activators (DMOG, DFO) or mesenchymal stem cells overexpressing HIF-1 α have been shown to improve fracture and bone defect healing [21–31].

The HIF- α signaling pathway might be involved in the pathogenesis of estrogen deficiency-induced osteoporosis. Our group reported that bone density, bone vessels, and bone formation were lower in *Hif1a* conditional knockout (KO) ovariectomized(OVX) mice than in wild-type OVX mice [32]. Moreover, the expression of HIF- α and VEGF decreased in OVX mice but not in *Vhl* KO OVX mice. In addition, *Vhl* KO OVX mice, which showed increased angiogenesis and osteogenesis due to activation of the HIF- α pathway, were protected from OVX-induced bone loss [33]. It has been suggested that 17 β -estradiol increases HIF-1 α and VEGF protein levels and partially stimulates human mesenchymal stem cell (hMSC) proliferation via HIF-1 α activation [34]. These data are consistent with the findings of Yen *et al.*, who demonstrated that diosgenin, which has estrogenic

effects, induces HIF-1 activation and angiogenesis through the src kinase, p38 MAPK, and Akt signaling pathways in osteoblasts [35]. Hence, decreased stimulation of the HIF-1 α pathway and angiogenesis might be important factors contributing to estrogen deficiency-induced bone loss. Therefore, activation of the HIF-1 α pathway might be a new approach to osteoporosis treatment.

In addition to affecting angiogenesis, hypoxia and hypoxia-mimicking agents increase osteogenesis and modulate Wnt/ β -catenin signaling [36]. Hypoxia promotes the proliferation of MSCs and accelerates their differentiation [37,38]. Similarly, overexpression of HIF-1 α in MSCs upregulates the mRNA and protein expression of osteogenic markers *in vitro* [24,25,39]. *In vivo* studies using transgenic mice have provided strong evidence that activation of HIF-1 α signaling in osteochondral progenitor cells or osteoprogenitor cells increases osteoblast proliferation and differentiation [18,19]. Treatment of MSCs/osteoblasts with DFO also increases osteogenic marker expression, the effect was attributed to activation of the Wnt/ β -catenin signaling pathways [40,41]. Two different groups have proposed that DMOG not only improves the angiogenic capacity of MSCs, but also enhances their osteogenic differentiation, though the exact mechanism has not been fully elucidated [21,30]. Considering that reduced osteogenesis of MSCs in postmenopausal women is a causative mechanism for osteoporosis, it is reasonable to promote osteogenesis by activation of the Wnt/ β -catenin pathway [42]. Therefore, Wnt/ β -catenin pathway stimulation might be a useful approach to osteoporosis treatment [43,44].

In light of their dual role in angiogenesis and osteogenesis, hypoxia-mimicking agents have tremendous potential for inhibiting bone loss. Supporting this notion, two recent studies have shown that activation of HIF-1 α signaling by DFO or inactivation of *Vhl* in osteochondral progenitor cells in a tamoxifen-inducible manner prevented age-induced bone loss [19,45]. However, iron overload has been regarded as a risk factor for postmenopausal osteoporosis [46,47]. To exclude the effect of “iron chelation” on the skeleton, we treated OVX mice with DMOG, a cell-permeable prolyl-4-hydroxylase inhibitor that stabilizes HIF-1 α under normal oxygen tension by suppressing PHD-mediated HIF-1 α degradation [14,16]. DMOG has shown promise as a therapeutic agent for bone defect healing, neuronal protection, diabetic wound healing, renal protection, and prevention of flap necrosis [21,30,48–55].

The present study was designed to assess the effect of DMOG on the skeleton of OVX mice by evaluating bone mass, bone microarchitecture, bone biomechanics, and bone turnover. Furthermore, the mechanism by which DMOG alters the HIF-1 α and Wnt/ β -catenin pathways was investigated.

Materials and Methods

Reagents and chemicals

All fine chemicals, including DMOG, tetracycline, dexamethasone, ascorbic acid, β -glycerophosphate, alizarin red S (ARS), 17 β -estradiol, L-glutamine, paraformaldehyde, ethylenediamine-tetraacetic acid (EDTA), 3-(5'-hydroxymethyl-2'-furyl)-1-benzyl indazole (YC-1), and the tartrate-resistant acid phosphatase staining kit (Leukocyte Acid Phosphatase Assay kit), were purchased from Sigma-Aldrich (St. Louis, MO, USA). Dulbecco's modified Eagle's medium (DMEM), fetal bovine serum (FBS), trypsin, penicillin-streptomycin, and TRIzol were purchased from Life Technologies (Gaithersburg, MD, USA). The mouse monoclonal antibodies for HIF-1 α and VEGF were purchased from Novus Biologicals (Littleton, CO, USA). The mouse monoclonal antibody for β -catenin was obtained from R&D Systems (Minneapolis, MN, USA), and the mouse monoclonal antibody for β -actin was

purchased from Anbo Biotechnology (San Francisco, CA, USA). The rabbit monoclonal antibody for T-cell factor 1 (TCF-1) was from Bioworld Technology, Inc. (St. Louis Park, MN, USA). The lymphoid enhancer-binding factor 1 (LEF-1) polyclonal antibody was obtained from Proteintech Group, Inc. (Chicago, IL, USA). The mouse monoclonal antibody for TATA-binding protein (TBP) was purchased from Abcam (Cambridge, UK). The goat anti-mouse and goat anti-rabbit secondary antibodies conjugated with horseradish peroxidase were purchased from Santa Cruz Biotechnology (Santa Cruz, CA, USA). The VEGF ELISA kit was purchased from R&D Systems (Minneapolis, MN, USA), the osteocalcin ELISA kit was from Biomedical Technologies, Inc. (Ward Hill, MA, USA), and the C-terminal telopeptides of collagen type(I) ELISA kit was from Immunodiagnostic Systems (Tyne&Wear, UK). The silicon rubber solution was purchased from Flow Tech (Microfil MV-122; Carver, MA, USA). The primers were synthesized by Invitrogen (Shanghai, China). The RevertAid First Strand cDNA Synthesis Kit was purchased from Thermo Fisher Scientific (Ottawa, Canada). SYBR Premix Ex Taq was purchased from TaKaRa Biotechnology (Dalian, China). The alkaline phosphatase staining (ALP) staining kit was purchased from Shanghai Rainbow Biotechnology (Shanghai, China). The BCA protein assay kit was purchased from Beyotime (Nantong, China). The eCL Western blot kit was obtained from CWBIO (Beijing, China).

Cell culture and treatment

Murine mesenchymal C3H10T1/2 clone 8 cells were obtained from the American Type Culture Collection (Rockville, MD, USA). The cells were cultured in DMEM supplemented with 10% FBS, 50 U/ml penicillin, 50 mg/ml streptomycin, and 4 mM L-glutamine. Cultures were incubated in a humidified incubator at 37°C and 5% CO₂. The cells were passaged every 3–4 days. The cells were then plated in 6-well plates at 1 × 10⁵ cells per well. After 24 hours, the cells were treated with the indicated concentrations of 17β-estradiol, DMOG, or DMOG+YC-1. For the hypoxia experiments, the cells were transferred into humidified incubators at 37°C with 5% CO₂, and the oxygen tension was reduced to 1% using supplemental N₂. In order to confirm the effect of DMOG on HIF-1α signaling pathway, the indicated treatment lasted 24 hours. For the experiment about exploration of DMOG on the differentiation of MSCs, the cells were cultured in osteogenic differentiation medium for 7 days. When treatment finished, the cells were collected for western blotting and quantitative real-time PCR analysis. The culture medium was collected for the measurement of VEGF by ELISA.

Quantitative real-time PCR for mRNA analysis

Total RNA from cells or bone samples were extracted using TRIzol reagent. In order to extract RNA from tibias, the tibias were grounded into pellets after the treatment with liquid nitrogen. cDNA was synthesized using 1 μg of RNA and a RevertAid First Strand cDNA Synthesis Kit. Gene expression was detected with real-time PCR using a SYBR Green qPCR kit and an ABI Step One Plus Real-Time PCR System. The primers used were listed in Table 1.

Western blot analysis

After cells or bone samples were lysed, the protein concentrations were measured using a BCA protein assay kit. Each protein sample (40 μg) was subjected to SDS electrophoresis and electroblotted onto a polyvinylidene difluoride membrane (0.45 μm; Millipore, Bedford, MA, USA). Afterwards, the membranes were blocked with 5% non-fat dry milk in Tris-buffered saline with

Tween 20 (TBST) for 1 hour. The membranes were probed with primary anti-HIF-1α (1:500), anti-TCF-1 (1:500), anti-LEF-1 (1:1000), anti-β-catenin (1:500), anti-TBP (1:2000), or anti-β-actin (1:5000) antibodies at 4°C overnight. The membranes were then washed three times with TBST and incubated for 1 hour with HRP-conjugated secondary antibodies (1:5000). The antigen-antibody complexes were visualized using the enhanced chemiluminescence detection system as recommended by the manufacturer.

Alkaline phosphatase staining and alizarin red staining

C3H10T1/2 cells were seeded onto 6-well plates at 1 × 10⁵ cells per well. After the cells reached confluence, the medium was changed to osteogenesis differentiation medium containing 10⁻⁷ M dexamethasone, 0.15 mM ascorbate-2-phosphate, and 2 mM β-glycerophosphate. The cells were cultured for 14 or 21 days and then subjected to ALP or ARS staining. The procedures were conducted according to established protocols. Briefly, the cells were washed with PBS (pH 7.4) three times and fixed with 4% paraformaldehyde (pH 7.4, dissolved in PBS) for 15 min. The cells were then stained with ALP reagent or 0.2% ARS solution for 30 min at 37°C, after which the cells were washed with deionized water three times. The ALP reagent was prepared according to the manufacturer's instructions.

Animal models

All animal care and experimental procedures were approved by the Institutional Animal Ethics Committee of Shanghai Ruijin Hospital (ethical approval number: 138). Two-month-old female C57BL/6J mice were obtained from Shanghai SLAC Laboratory Animal Co., Ltd (Shanghai, China). The mice were housed five per cage and were maintained under a strict 12-h light:12-h dark cycle at 22°C with standard food pellets and free access to tap water. After a 2-week adaptation, ten-week-old mice were randomly divided into four groups as follows: sham group (ovary intact+vehicle (normal saline) i.p.), OVX group (OVX+vehicle), OVX+L-DMOG group (OVX+5 mg/kg/day DMOG i.p.), and OVX+H-DMOG group (OVX+20 mg/kg/day DMOG i.p.). The ovariectomy was performed in a surgery room exposed to ultraviolet radiation overnight. After anesthetization, the bilateral ovaries were exposed and removed from OVX animals; in the sham animals, the ovaries were exposed but left intact. After surgery, each mouse received an i.p. injection of gentamicin (1000 U) for three successive days. In order to confirm the successful establishment of OVX model, the femoral BMD of 8 mice were measured by *in vitro* micro computed tomography (micro-CT) before the surgery, and the BMD of another 8 mice were assessed one month later. The mice were sacrificed by anesthetic overdose. The uterus of each mouse was isolated and weighed. The body weight of each mouse was recorded. The femurs were collected for micro-CT, histological analyses and mechanical test. The left tibia of each mouse was used for PCR analysis, and the right tibia was used for western blot analysis.

Analysis of micro-CT scans

The distal metaphysis right femur were scanned with a high-resolution (8 μm) micro-CT scanner (GE eXplore Locus SP) to evaluate bone mass, geometry, and trabecular microarchitecture. The parameters computed from these data included bone mineral density (BMD), bone volume/tissue volume (BV/TV), trabecular thickness (Tb.Th), trabecular number (Tb.N), and trabecular separation (Tb.Sp).

Table 1. Primers for Real-time PCR analysis.

Gene	Forward Premier	Reverse Premier
VEGF	5'-GGCTCTGAAACCATGAACCTTCT-3'	5'-GCAGTAGCTGCGCTGGTAGAC-3'
β -catenin	5'-GGAAAGCAAGCTCATCTTCT-3'	5'-AGTGCCTGCATCCACCA-3'
Runx-2	5'-GTGCTACTGCGCTGAAGAGG-3'	5'-GACCAACCGAGTCATTTAAGGC-3'
Osterix	5'-ACCAGGTCCAGGCAACAC-3'	5'-GCAGTCGCAGGTAGAACG-3'
ALP	5'-ACGAGATGCCACCAGAGG-3'	5'-AGTTCAGTVCGGTCCAG-3'
Osteocalcin	5'-TGCTACTCTGCTGACCCTG-3'	5'-TTATTGCCCTCTGCTTG-3'
RANKL	5'-CGTACCTGCGGACTATCTTCA-3'	5'-CTTGGACACCTGGACGCTAA-3'
OPG	5'-CATCGAAAGCACCTGTA-3'	5'-CACTACGCCAATTCGGTAT-3'
β -actin	5'-CCCTGTATGCCTCTGGTC-3'	5'-GCTTTACGGATGTCAACG-3'

doi:10.1371/journal.pone.0112744.t001

Mechanical testing

The femora from the mice were wrapped in medical gauze saturated with normal saline and stored at 4°C for use the next day. Before testing, the samples were brought to room temperature for 1 hour. The three-point bending test of the left femur was carried out using an Instron 5569 materials testing machine (Instron Inc., Norwood, MA, USA). The femur was placed posterior side down between two supports, which were 6 mm apart. A load was applied at the mid-span, which bent the bone about the anteroposterior axis. Load-displacement curves were recorded at a crosshead speed of 1 mm/s.

Imaging of femoral blood vessels

Specimens were prepared as previously reported [33]. Briefly, after the mice were euthanized, the thoracic cavity was opened, and the inferior vena cava was dissected and flushed with 0.9% normal saline containing heparin sodium (100 U/ml) to remove the blood from the vessels. Afterwards, the vasculature was perfused with 10% neutral buffered formalin. The vasculature was then injected with 5 ml of silicone rubber compound. Sufficient perfusion was defined as a yellow color change in the lower limbs and liver. The specimens were stored at 4°C overnight, after which the femora were dissected and fixed in 4% paraformaldehyde for an additional 48 hours. The femora were then decalcified in 10% EDTA for four weeks. Images were obtained with a high-resolution (isotropic voxel size of 16 μ m) micro-CT imaging system. A threshold of 100 was chosen, and the vessel volume within a region of 5 mm beginning from the distal end of the femur was evaluated.

Histological preparation and tartrate-resistant acid phosphatase staining

The specimens were decalcified in 10% EDTA for four weeks, and the EDTA solution was changed twice a week. The bones were then dehydrated in a graded series of ethanol washes from 70%–100% before embedding the samples in paraffin. Five-micron-thick longitudinal serial sections were cut and mounted on poly-lysine-coated slides. The deparaffinized slides were washed with PBS three times. The slides were then incubated at 37°C for 60 min in the dark in a solution containing sodium nitrite, fast garnet, naphthol AS-BI phosphoric acid, acetate, and tartrate from the Leukocyte Acid Phosphatase Assay kit, according to the manufacturer's instructions. Finally, the nuclei were counterstained with methyl green. Multinucleated cells with three or more nuclei were scored as osteoclasts. The average number of

osteoclasts per mm of bone surface was then calculated for each femur.

Fluorochrome labeling and bone histomorphometry

A double tetracycline (25 mg/kg) label was injected subcutaneously at 10 and 3 days before necropsy. At necropsy, the femora were cleaned of soft tissue and fixed in 70% ethanol. The bones were dehydrated and embedded in methyl methacrylate. Thin frontal sections of the femur (5 μ m) were cut using a microtome (Leica RM2255). Bone histomorphometric parameters were determined according to the report of the American Society of Bone and Mineral Research Nomenclature Committee [56]. Histomorphometric measurements included single-labeled surface (sLS), double-labeled surface (dLS), and interlabel thickness (IrLTh). These data were used to calculate the mineralizing surface/bone surface ratio (MS/BS), mineral apposition rate (MAR), and bone formation rate (BFR) as follows: $MS/BS = (1/2sLS + dLS)/BS(\%)$, $MAR = Ir.L.Th/Ir.L.t$, and $BFR/BS = MAR \times MS/BS (m^3/m^2/day)$.

Enzyme-linked immunosorbent assay

Blood from the mice was collected, and the serum was separated by centrifugation at 3000 rpm for 30 min. Serum VEGF, osteocalcin, and CTX levels were measured by ELISA, following the manufacturers' protocols.

Statistical analysis

The results were expressed as the mean \pm SD. All experimental data were analyzed with one-way analysis of variance (ANOVA) followed by Duncan's test. $P < 0.05$ was considered statistically significant.

Results

Effect of 17 β -estradiol and DMOG on the HIF-1 α signaling pathway

Consistent with previous reports, our western blot analysis showed that 17 β -estradiol stabilized HIF-1 α under normal oxygen tension (Fig. 1A). Furthermore, 17 β -estradiol increased the expression of VEGF protein (control vs. $10^{-9}E_2$ $P = 0.001 < 0.05$, control vs. $10^{-7}E_2$ $P = 0.000 < 0.05$, control vs. $10^{-5}E_2$ $P = 0.000 < 0.05$), the main downstream angiogenic target of the HIF-1 α pathway, in a dose-dependent manner (Fig. 1B). Similarly, DMOG enhanced HIF-1 α protein expression under normal

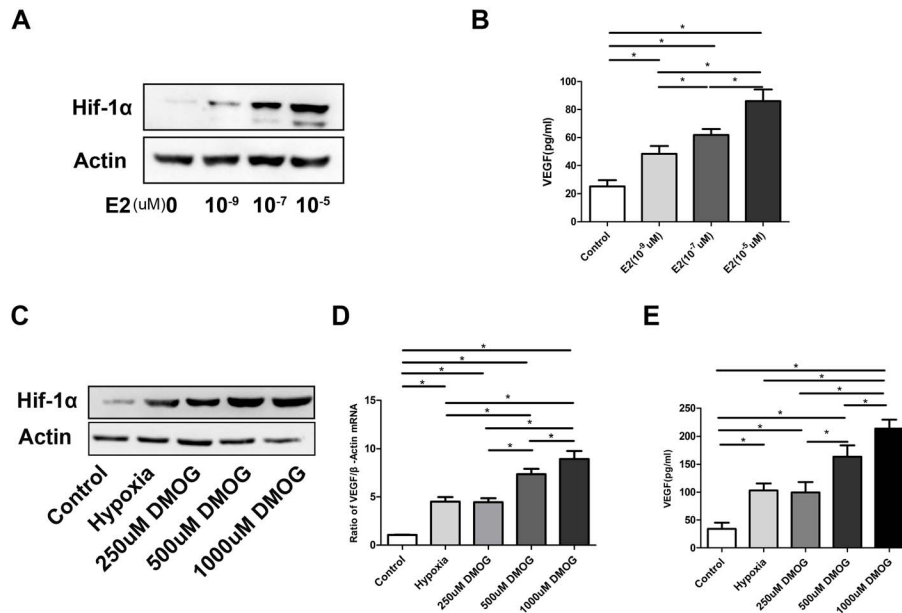


Figure 1. Effect of 17β-estradiol and DMOG on HIF-1α signaling pathway. (A) 17β-estradiol stabilized HIF-1α under normal oxygen pressure. (B) 17β-estradiol upregulated VEGF protein expression. (C) DMOG enhanced HIF-1α protein expression. (D–E) DMOG upregulated VEGF expression at the mRNA and protein levels. $P < 0.05$ for comparisons among the groups designated with an asterisk. doi:10.1371/journal.pone.0112744.g001

oxygen tension and upregulated VEGF expression at the mRNA and protein levels (Fig. 1C–E).

Effect of DMOG on MSC osteogenic differentiation and the Wnt/β-catenin signaling pathway

ALP and ARS staining showed that DMOG treatment enhanced osteogenic differentiation and calcium deposition (Fig. 2A). Consistent with osteogenesis, RUNX-2 and osterix mRNA levels were increased (RUNX-2 $P = 0.000 < 0.05$, osterix $P = 0.000 < 0.05$) (Fig. 2B). Investigation into the underlying mechanism revealed that DMOG upregulated the levels of β-catenin mRNA and protein ($P = 0.000 < 0.05$) (Fig. 2C). To determine whether the effect of DMOG on Wnt/β-catenin signaling was mediated by HIF-1α signaling, we treated MSCs with YC-1, a widely used HIF-1α inhibitor, along with DMOG and assessed the nuclear expression of β-catenin and the downstream effectors LEF-1 and TCF-1. DMOG stimulated HIF-1α protein expression, and YC-1 inhibited the effect of DMOG on HIF-1α. Furthermore, YC-1 attenuated the DMOG-induced increase in nuclear β-catenin, LEF-1, and TCF-1 protein expression (Fig. 2D).

Confirmation of the OVX model

OVX increased body weight by approximately 6% when compared to sham treatment (Sham vs. OVX $P = 0.049 < 0.05$). However, DMOG treatment did not affect the OVX-induced body weight gain (OVX+L-DMOG vs. OVX $P = 0.868 > 0.05$, OVX+H-DMOG vs. OVX $P = 1.000 > 0.05$) (Fig. S1A). The efficacy of OVX was confirmed by changes in uterine and BMD. The average uterine weights in each group were 0.11137 ± 0.0120 g (sham), 0.0319 ± 0.0079 g (OVX), 0.0337 ± 0.079 g (OVX+L-DMOG), and 0.0326 ± 0.0078 g (OVX+H-DMOG) ($P < 0.0001$) (Fig. S1B,C). Before ovariectomy, the BMD of mice was 365.41 ± 18.43 mg/cm³, and OVX made the BMD of mice decrease to 281.26 ± 29.61 mg/cm³ ($P < 0.0001$) (Fig. S1D).

The effect of DMOG on BMD, bone microarchitecture, and vessels

To characterize the effects of treatment on the trabecular bone compartments, the distal metaphysis of the femoral bone was evaluated with micro-CT imaging (Table. 2). With regard to trabecular bone alterations, OVX mice showed remarkable reductions in BMD, BV/TV, Tb.N, and Tb.Th, as well as increased Tb.Sp (OVX vs. Sham: BMD $P = 0.000 < 0.05$, BV/TV $P = 0.000 < 0.05$, Tb.N $P = 0.000 < 0.05$, Tb.Th $P = 0.005 < 0.05$, Tb.Sp $P = 0.000 < 0.05$). DMOG treatment, especially at high doses, improved the trabecular microarchitecture and increased BMD (OVX vs. OVX+L-DMOG: BMD $P = 0.025 < 0.05$, BV/TV $P = 0.184 > 0.05$, Tb.N $P = 0.019 < 0.05$, Tb.Th $P = 0.94 > 0.05$, Tb.Sp $P = 0.191 > 0.05$; OVX vs. OVX+H-DMOG: BMD $P = 0.000 < 0.05$, BV/TV $P = 0.000 < 0.05$, Tb.N $P = 0.000 < 0.05$, Tb.Th $P = 0.047 < 0.05$, Tb.Sp $P = 0.016 < 0.05$) (Fig. 3A). Microfil-perfused femora were analyzed with micro-CT to assess vascularity. The number of blood vessels in the femur was lower 4 weeks after OVX ($P = 0.000 < 0.05$). However, DMOG treatment led to a dose-dependent increase in femur vessel volume relative to that in the OVX group (OVX vs. OVX+L-DMOG $P = 0.045 < 0.05$, OVX vs. OVX+H-DMOG $P = 0.000 < 0.05$), although differences among the DMOG-treated groups and the sham group were evident (Sham vs. OVX+L-DMOG $P = 0.000 < 0.05$, Sham vs. OVX+H-DMOG $P = 0.009 < 0.05$) (Fig. 3B).

Bone mechanical strength examination

The three-point bending test was used to evaluate bone strength (Table. 3). The femurs of the OVX mice exhibited decreases in ultimate stress, ultimate load, energy to failure, and modulus, all of which reflected a decline in bone strength following OVX (Sham vs. OVX: ultimate stress $P = 0.000 < 0.05$, ultimate load $P = 0.000 < 0.05$, energy to failure $P = 0.000 < 0.05$, modulus $P = 0.000 < 0.05$). DMOG treatment improved ultimate stress, ultimate load, energy to failure, and modulus (OVX vs. OVX+L-DMOG: ultimate stress $P = 0.010 < 0.05$, ultimate load

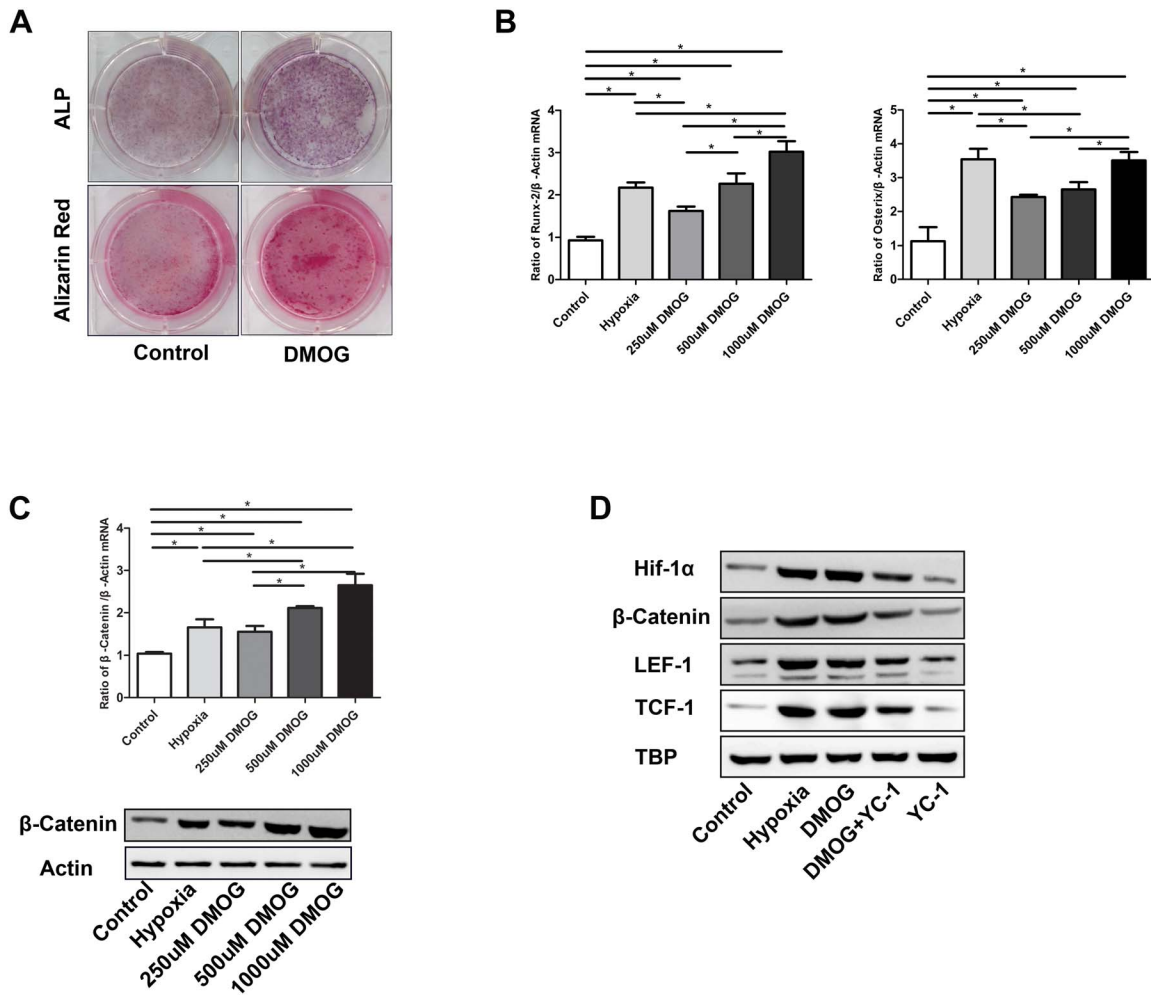


Figure 2. Effect of DMOG on MSC osteogenic differentiation and Wnt/ β -catenin signaling. (A) ALP and alizarin red S staining. (B) DMOG promoted RUNX-2 and osterix mRNA expression. (C) DMOG increased β -catenin mRNA and protein expression. (D) DMOG increased nuclear β -catenin, LEF-1, TCF-1, and HIF-1 α protein expression. These effects were attenuated by YC-1. $P < 0.05$ for comparisons among the groups designated with an asterisk.

doi:10.1371/journal.pone.0112744.g002

$P = 0.005 < 0.05$, energy to failure $P = 0.024 < 0.05$, modulus $P = 0.051 > 0.05$; OVX vs. OVX+H-DMOG ultimate stress $P = 0.000 < 0.05$, ultimate load $P = 0.000 < 0.05$, energy to failure $P = 0.001 < 0.05$, modulus $P = 0.009 < 0.05$).

Serum VEGF, osteocalcin, and CTX levels

The serum level of VEGF, the main angiogenic cytokine upregulated by HIF-1 α , was markedly reduced in OVX mice ($P = 0.000 < 0.05$), and DMOG treatment improved VEGF levels in a dose-dependent manner (OVX vs. OVX+L-DMOG $P = 0.003 < 0.05$, OVX vs. OVX+H-DMOG $P = 0.000 < 0.05$).

Table 2. Micro-CT analysis of trabecular BMD, bone microarchitecture and vasculature in the distal femur.

	Sham	OVX	OVX+L-DMOG	OVX+H-DMOG
BMD(mg/cm ³)	379.69 ± 24.61 [#]	284.46 ± 17.49*	309.10 ± 19.03* [#]	335.62 ± 30.94* [#]
BV/TV(%)	0.1331 ± 0.0061 [#]	0.0947 ± 0.0139*	0.1013 ± 0.0105*	0.1143 ± 0.0119* [#]
Tb.N(1/mm)	3.7268 ± 0.2478 [#]	2.5724 ± 0.4024*	2.9317 ± 0.2273* [#]	3.3250 ± 0.3884* [#]
Tb.Th(um)	0.0345 ± 0.0013 [#]	0.0322 ± 0.0014*	0.0323 ± 0.0109*	0.0339 ± 0.0025 [#]
Tb.Sp(um)	0.2351 ± 0.0211 [#]	0.3033 ± 0.0379*	0.2854 ± 0.0183*	0.2693 ± 0.0371* [#]
Vessel volume(mm ³)	0.4441 ± 0.0396 [#]	0.2189 ± 0.0419*	0.2766 ± 0.0243* [#]	0.3529 ± 0.0315* [#]

The groups designated with an asterisk shown significant differences with Sham group ($P < 0.05$), the groups designated with a pound sign shown significant differences with OVX group ($P < 0.05$).

doi:10.1371/journal.pone.0112744.t002

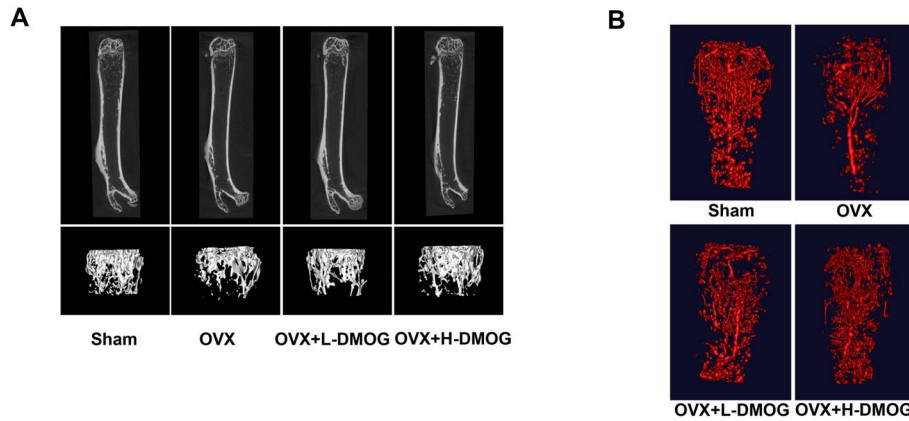


Figure 3. BMD and bone microarchitecture of the trabecular bone in the distal femur. (A) DMOG abrogated the decrease in BMD and the deterioration in bone microarchitecture induced by OVX, as measured by micro-CT. **Morphological analysis of the vasculature within the distal femur from Microfil-perfused mice.** (B) OVX decreased the vessel volume at the distal metaphysis of the femur, while DMOG treatment partly restored vessel volumes.
doi:10.1371/journal.pone.0112744.g003

Serum osteocalcin, a marker for bone formation, was higher in OVX mice than in sham mice, but the difference was not significant ($P = 0.053 > 0.05$). The osteocalcin levels in the DMOG-treated group were significantly higher than those in the OVX group (OVX vs. OVX+L-DMOG $P = 0.008 < 0.05$, OVX vs. OVX+H-DMOG $P = 0.000 < 0.05$). Serum CTX, a marker of bone resorption, was approximately two-fold higher in OVX mice than in sham mice ($P = 0.000 < 0.05$), while DMOG treatment did not affect serum CTX levels (OVX vs. OVX+L-DMOG $P = 0.714 > 0.05$, OVX vs. OVX+H-DMOG $P = 0.770 > 0.05$). All the data were listed in Table 4.

Osteoclast number

Consistent with the results of the serum CTX analysis, the TRAP assay revealed a striking increase in osteoclast number following OVX (5.200 ± 0.836 and 13.200 ± 1.303 in the sham group and OVX group, respectively ($P = 0.000 < 0.05$)). DMOG administration did not noticeably prevent OVX-induced osteoclast formation (12.800 ± 1.643 in the OVX+L-DMOG group and 12.600 ± 2.673 in OVX+H-DMOG group; OVX+L-DMOG vs. the OVX group $P = 1.000 > 0.05$, OVX+H-DMOG vs. the OVX group $P = 0.637 > 0.05$) (Fig. 4A).

Dynamic bone histomorphometry

The dynamic histology of the trabecular bone in the distal femur was compared among the various groups. OVX resulted in significant increases in MS/BS and BFR/BS (Sham vs. OVX: MS/BS $P = 0.000 < 0.05$, BFR/BS $P = 0.004 < 0.05$) and increased

MAR though without statistical difference ($P = 0.057 > 0.05$). H-DMOG treatment further increased MS/BS, MAR, and BFR/BS compared with OVX group (MS/BS $P = 0.000 < 0.05$, MAR $P = 0.001 < 0.05$, BFR/BS $P = 0.000 < 0.05$); and L-DMOG administration increased MAR and BFR/BS (MAR $P = 0.035 < 0.05$, BFR/BS $P = 0.000 < 0.05$) but not MS/BS ($P = 0.061 > 0.05$) compared to OVX group (Fig. 4B).

Alterations in HIF-1 α and Wnt/ β -catenin signaling in DMOG-treated mice

To illustrate the enhanced angiogenesis and osteogenesis in DMOG-treated mice, we used western blot to detect alterations in HIF-1 α and Wnt/ β -catenin signaling pathways in collected bone samples (Fig. 5A). As previously highlighted, OVX substantially reduced HIF-1 α expression; the reduction in HIF-1 α was accompanied by a decrease in VEGF expression. However, in the DMOG-treated group, the expression of HIF-1 α and VEGF increased significantly. Moreover, DMOG administration enhanced β -catenin expression relative to expression in the OVX group.

Bone formation and bone resorption markers in DMOG-treated mice

Real-time PCR results for ALP, osteocalcin, RUNX-2, RANKL, OPG, and β -actin expression in each group are shown in Fig. 5B. OVX increased ALP, osteocalcin, and RUNX-2 mRNA levels over those in the sham group, but the difference was not statistically significant (ALP $P = 0.262 > 0.05$, osteocalcin

Table 3. Bone quality of the femur as measured by the three-point bending test.

	Sham	OVX	OVX+L-DMOG	OVX+H-DMOG
Ultimate load(N)	15.31±0.85 [#]	11.85±0.30*	13.14±0.42* [#]	14.11±0.37* [#]
Ultimate stress(Mpa)	99.41±7.10 [#]	69.56±4.88*	80.98±5.59* [#]	90.13±2.37* [#]
Energy to failure(MJ)	8.69±0.50 [#]	6.75±0.24*	7.39±0.30* [#]	7.92±0.31* [#]
Modulus(Mpa)	4162.65±377.13 [#]	2910.93±355.07*	3407.78±291.51*	3624.83±255.12* [#]

The groups designated with an asterisk shown significant differences with Sham group ($P < 0.05$), the groups designated with a pound sign shown significant differences with OVX group ($P < 0.05$).

doi:10.1371/journal.pone.0112744.t003

Table 4. Biochemical markers of bone in serum as measured by ELISA.

	Sham	OVX	OVX+L-DMOG	OVX+H-DMOG
VEGF(pg/ml)	116.37±6.21#	82.37±8.90*	93.13±5.51*#	100.75±5.31*#
Osteocalcin(ng/ml)	68.33±14.22	80.80±18.87	98.32±9.95*#	107.60±10.91*#
CTX(ng/ml)	16.21±1.61	28.01±1.95*	28.46±4.35*	27.65±2.10*

The groups designated with an asterisk shown significant differences with Sham group ($P < 0.05$), the groups designated with a pound sign shown significant differences with OVX group ($P < 0.05$).

doi:10.1371/journal.pone.0112744.t004

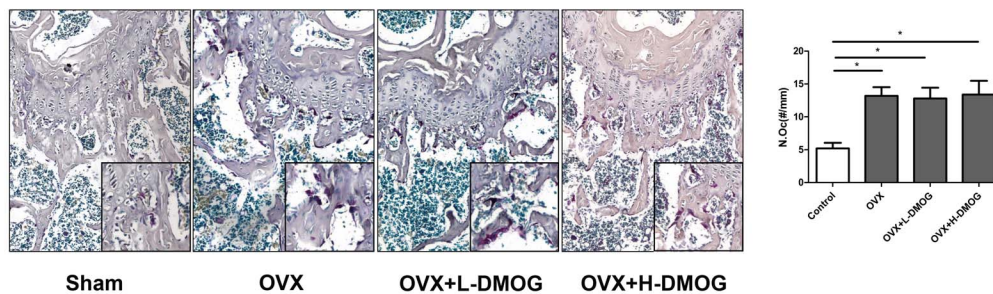
$P = 0.089 > 0.05$, $RUNX-2 P = 0.346 > 0.05$). The osteocalcin mRNA level was higher in the DMOG-treated OVX groups than in the OVX groups (OVX vs. OVX+L-DMOG $P = 0.030 < 0.05$, OVX vs. OVX+H-DMOG $P = 0.000 < 0.05$), and ALP and $RUNX-2$ mRNA levels were markedly higher in the H-DMOG treated group than in the OVX group (ALP $P = 0.001 < 0.05$, $RUNX-2 P = 0.004 < 0.05$). In OVX mice, RANKL/OPG expression was markedly increased when compared with expression in the sham group ($P = 0.006 < 0.05$). However, DMOG administration did not significantly attenuate the OVX-induced

increase in RANKL/OPG expression (OVX vs. OVX+L-DMOG $P = 0.733 > 0.05$, OVX vs. OVX+H-DMOG $P = 0.984 > 0.05$).

Discussion

In the present study, DMOG improved angiogenesis and osteogenesis *in vitro*. The effects were attributed to activation of the HIF-1 α and Wnt/ β -catenin signaling pathways, respectively. We investigated whether DMOG ameliorated OVX-induced osteoporosis in mice. Our results showed that DMOG improved BMD, trabecular microarchitecture, and bone strength in OVX mice. In addition, DMOG treatment partly restored the blood

A



B

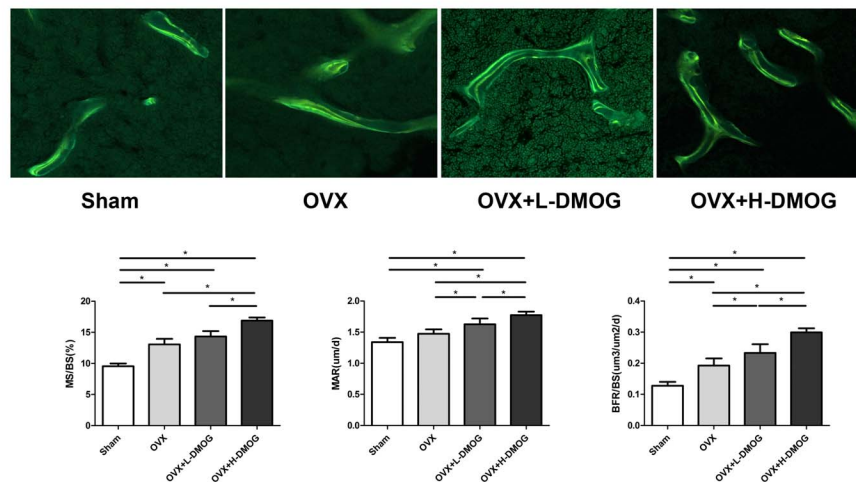


Figure 4. Osteoclast numbers assayed by tartrate-resistant acid phosphatase staining of femoral sections. (A) Osteoclast counting results showed that DMOG treatment had no obvious effect on OVX-enhanced osteoclast formation. Original magnification, $\times 100$. **Dynamic bone formation illustrated by double tetracycline labeling. (B)** DMOG administration promoted bone formation, as evidenced by improved MS/BS, MAR, and BFR/BS. Original magnification, $\times 200$. $P < 0.05$ for comparisons among the groups designated with an asterisk.

doi:10.1371/journal.pone.0112744.g004

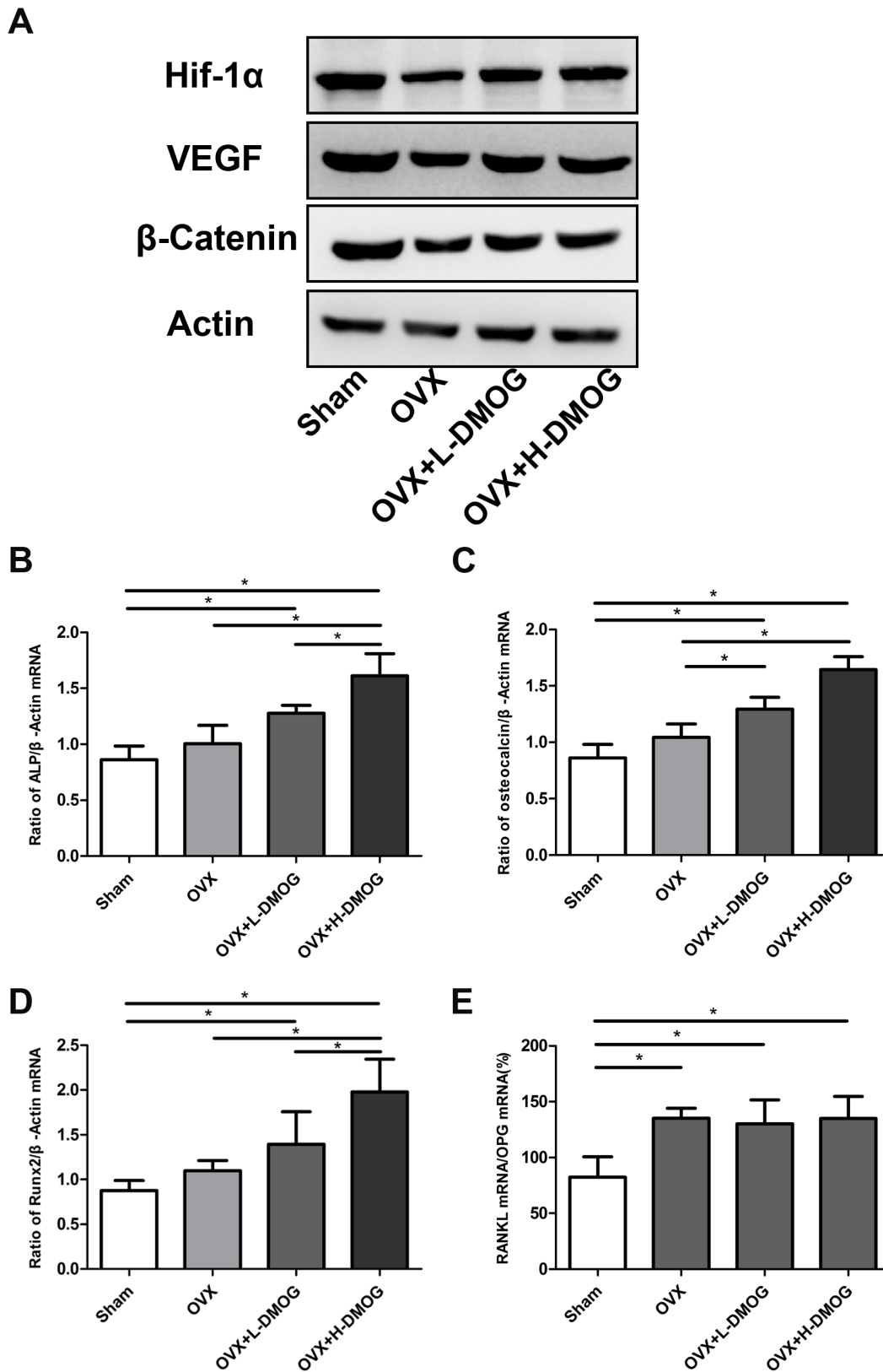


Figure 5. HIF-1α, VEGF, and β-catenin expression in bone samples detected by western blot. (A) HIF-1α, VEGF, and β-catenin expression was lower in OVX mice than in sham mice. However, DMOG treatment increased HIF-1α, VEGF, and β-catenin expression relative to expression in the OVX group. **Effects of DMOG administration on tibial ALP, osteocalcin, RUNX-2, and RANKL/OPG mRNA expression in OVX mice assessed by real-time PCR.** (B) ALP/β-actin ratio. (C) Osteocalcin/β-actin ratio. (D) RUNX-2/β-actin ratio. (E) RANKL/OPG/β-actin ratio. *P*<0.05 for comparisons among the groups designated with an asterisk. doi:10.1371/journal.pone.0112744.g005

vessels of OVX mice. Enhanced osteogenesis might underlie these improvements, as indicated by the acceleration in MS/BS, BFR/BS, and MAR; the increase in serum osteocalcin; and the upregulation of tibial ALP, osteocalcin, and RUNX-2 mRNA. In addition, significant remediation of angiogenesis resulting from increases in VEGF also led to improved bone health in OVX mice.

Stimuli other than hypoxia also cause HIF-1 α to accumulate in normoxic cells. For example, growth factors such as insulin-like growth factor can induce HIF-1 α synthesis through activation of the PI3 K/Akt/mTOR signal transduction pathway [57,58]. Here, we found that 17 β -estradiol stabilized HIF-1 α under normal oxygen tension and increased VEGF protein expression, consistent with previous reports [34,35]. This phenomenon explains our previous finding that OVX decreased HIF-1 α and VEGF expression in osteoblasts [33]. Impaired regulation of HIF-1 α is also observed in other pathological processes, such as the development of diabetic wounds, and stabilization of HIF-1 α is pivotal for reversing these pathological processes [59]. Mice in which HIF-1 α signaling was activated developed extremely dense, heavily vascularized bones, and these mice were protected from OVX or age-induced bone loss [19,33]. More importantly, age-related bone loss has been prevented by administration of DFO, a hypoxia-mimicking agent [45]. Therefore, stabilization of HIF-1 α by a hypoxia-mimicking agent might also help prevent estrogen deficiency-induced bone loss. Another widely used hypoxia-mimicking agent, DMOG, modulated VEGF mRNA and protein levels, which were mainly associated with activated HIF-1 α under normal oxygen pressure [14,16,20].

In addition to its angiogenic effects, DMOG also has potent osteogenic effects. Enhanced osteogenic differentiation of DMOG-treated MSCs was demonstrated by ALP staining and calcium deposition, which are early and late stage osteogenic markers, respectively. To characterize the underlying molecular mechanism, alterations in the mRNA levels of RUNX-2 and osterix, essential transcription factors for the differentiation of osteoblasts from MSCs [60], were assessed. Our results and those of two recent studies indicate that DMOG upregulates RUNX-2 and osterix mRNA expression [21,30]. These results were supported by the finding that osteogenesis was enhanced in MSCs expressing a constitutively active form of HIF-1 α [24,25,39]. Osteoblastic differentiation is predominantly regulated by the Wnt/ β -catenin signaling pathway. Wnt binds to Frizzled receptors and their co-receptors, low-density lipoprotein receptor-related proteins (LRP5/6), to stabilize cytosolic β -catenin. β -Catenin then enters the nucleus and stimulates the transcription of Wnt target genes [61]. A reduction in serum β -catenin might contribute to the pathogenesis of postmenopausal osteoporosis [62]. In our studies, DMOG upregulated β -catenin mRNA and protein expression in a dose-dependent manner. Our findings are consistent with those of other groups, which showed that hypoxia and hypoxia mimetics, such as DFO, increase Wnt/ β -catenin signaling in MSCs and osteoblasts [40,41]. As for the relationship between HIF-1 α signaling and Wnt/ β -catenin signaling, a previous study showed that HIF-1 α modulated Wnt/ β -catenin signaling in embryonic stem cells [36]. Our studies showed that this phenomenon occurs in MSCs. DMOG increased the expression of nuclear β -catenin and the downstream effectors LEF-1 and TCF-1. The effects were abrogated by the HIF-1 α signaling inhibitor YC-1 [63–66]. These results suggest that the effect of DMOG on Wnt/ β -catenin signaling is mediated by HIF-1 α signaling.

In view of the dual role of DMOG in angiogenesis and osteogenesis, we hypothesized that DMOG would attenuate bone loss in OVX mice. As expected, DMOG administration increased

the BMD of the trabecular bone. In addition to the BMD, the bone microarchitecture is a critical factor commonly associated with bone quality. Our results showed that BV/TV, Tb.N, Tb.Th, and Tb.Sp, the four fundamental indices of trabecular architecture as determined by the American Society for Bone and Mineral Research, were partly restored to differing extents by DMOG treatment, especially in the H-DMOG-treated group [67]. Because both bone mineral density and microarchitecture, two important factors that determine bone quality, improved significantly, we tested bone strength using the three-point bending test, which showed that DMOG treatment partly rescued the decline in bone mechanical strength due to OVX. These findings strongly suggest that DMOG prevents bone loss and improves bone quality in OVX mice.

Given that angiogenesis and osteogenesis are closely coupled, multiple studies have investigated the role of angiogenesis in the pathogenesis of osteoporosis. Accumulating evidence from studies in cells, animals, and patients indicates that low estrogen levels contribute to fewer vessels or decreases in angiogenic factors, resulting in the progression of osteoporosis [4–11]. Our current study supports this idea. OVX decreased the femoral vessel volumes of OVX mice, but femoral vessel volumes were partly restored in the DMOG-treated groups. The alteration in bone vessel volumes was in accordance with that of bone parameters. Furthermore, the restoration of bone vessel volume was coincident with the increased expression of HIF-1 α and VEGF in bone samples. VEGF, the best known and most critical angiogenic factor, induces vessel formation and regulates the balance between osteogenic and adipogenic differentiation in MSCs. Mice with VEGF deficiency in osteoblastic precursor cells exhibited an osteoporosis-like phenotype characterized by reduced bone mass and increased bone marrow fat content [68]. Hence, normalization of low VEGF levels in postmenopausal women might be of critical significance.

Compared with antiresorptive drugs, which excessively reduce bone turnover and result in inadequate microdamage repair, drugs targeted towards impaired bone formation might be better suited to the rehabilitation of osteoporotic bone [69]. Our *in vivo* data, including serum osteocalcin, real-time PCR, and dynamic bone histomorphometry results, indicated that DMOG administration further increased osteogenesis in OVX mice [60]. These results are consistent with findings that inactivation of *Vhl* in osteochondral progenitor cells or osteoprogenitor cells increases the proliferation and differentiation of osteoblast lineage cells *in vivo* [18,19]. Furthermore, the expression of osteoprogenitor and osteoblast markers, including osterix, bone γ -carboxyglutamate protein, and integrin-binding sialoprotein, increased in the long bone of DFO-treated aged mice [45]. The enhanced differentiation of osteoblasts was probably attributed to elevated β -catenin protein expression, which was confirmed by western blot. In addition to the regulation of the Wnt/ β -catenin pathway by HIF-1 α signaling, demonstrated *in vitro* in this study, the increased level of VEGF might be another pivotal factor for β -catenin accumulation [70]. Although it has been suggested that activation of the Wnt/ β -catenin pathway decreases bone resorption, we did not detect a significant alteration in bone resorption following DMOG treatment, as shown by the serum CTX levels and the osteoclast numbers in the femur [71,72].

There were several limitations to this study: 1) the BMD and microarchitecture of the lumbar vertebra were not assessed; 2) it would be better if the treatment lasts longer time.

Conclusions

The results of present study demonstrate that DMOG treatment prevents bone loss, rescues bone microarchitecture deterioration, and restores bone strength in OVX mice. The effects might result from enhanced angiogenesis and osteogenesis. Following DMOG administration, new vessel formation, induced by angiogenic factors, would supply the bone with oxygen, nutrients, and a variety of cells, especially MSCs. Activation of the Wnt/ β -catenin signaling pathway would enhance the osteogenic differentiation of MSCs and promote bone formation. To the best of our knowledge, this is the first report to describe the use and dual role of DMOG in the treatment of OVX-induced osteoporosis. DMOG may be a new strategy for the treatment of postmenopausal osteoporosis.

Supporting Information

Figure S1 Body weight, uterus weight, representative picture of uterus in each group and BMD alterations before and after OVX. (A) OVX significantly increased body

References

- Kanis JA (1994) Assessment of fracture risk and its application to screening for postmenopausal osteoporosis: synopsis of a WHO report. WHO Study Group. *Osteoporos Int* 4: 368–381.
- Qu B, Ma Y, Yan M, Wu HH, Fan L, et al. (2014) The economic burden of fracture patients with osteoporosis in western China. *Osteoporos Int* 25: 1853–1860.
- Brandi ML, Collin-Osdoby P (2006) Vascular biology and the skeleton. *J Bone Miner Res* 21: 183–192.
- Mekraldi S, Lafage-Proust MH, Bloomfield S, Alexandre C, Vico L (2003) Changes in vasoactive factors associated with altered vessel morphology in the tibial metaphysis during ovariectomy-induced bone loss in rats. *Bone* 32: 630–641.
- Ding WG, Wei ZX, Liu JB (2011) Reduced local blood supply to the tibial metaphysis is associated with ovariectomy-induced osteoporosis in mice. *Connect Tissue Res* 52: 25–29.
- Vogt MT, Cauley JA, Kuller LH, Nevitt MC (1997) Bone mineral density and blood flow to the lower extremities: the study of osteoporotic fractures. *J Bone Miner Res* 12: 283–289.
- Griffith JF, Wang YX, Zhou H, Kwong WH, Wong WT, et al. (2010) Reduced bone perfusion in osteoporosis: likely causes in an ovariectomy rat model. *Radiology* 254: 739–746.
- Shih TT, Liu HC, Chang CJ, Wei SY, Shen LC, et al. (2004) Correlation of MR lumbar spine bone marrow perfusion with bone mineral density in female subjects. *Radiology* 233: 121–128.
- Senel K, Baykal T, Seferoglu B, Altas EU, Baygutalp F, et al. (2013) Circulating vascular endothelial growth factor concentrations in patients with postmenopausal osteoporosis. *Arch Med Sci* 9: 709–712.
- Mueller MD, Vigne JL, Minchenko A, Lebovic DI, Leitman DC, et al. (2000) Regulation of vascular endothelial growth factor (VEGF) gene transcription by estrogen receptors alpha and beta. *Proc Natl Acad Sci U S A* 97: 10972–10977.
- Pufe T, Claassen H, Scholz-Ahrens KE, Varoga D, Drescher W, et al. (2007) Influence of estradiol on vascular endothelial growth factor expression in bone: a study in Gottingen miniature pigs and human osteoblasts. *Calcif Tissue Int* 80: 184–191.
- Min JH, Yang H, Ivan M, Gertler F, Kaelin WG Jr, et al. (2002) Structure of an HIF-1 α -pVHL complex: hydroxyproline recognition in signaling. *Science* 296: 1886–1889.
- Maxwell PH, Wiesener MS, Chang GW, Clifford SC, Vaux EC, et al. (1999) The tumour suppressor protein VHL targets hypoxia-inducible factors for oxygen-dependent proteolysis. *Nature* 399: 271–275.
- Jaakkola P, Mole DR, Tian YM, Wilson MI, Gielbert J, et al. (2001) Targeting of HIF-1 α to the von Hippel-Lindau ubiquitylation complex by O₂-regulated prolyl hydroxylation. *Science* 292: 468–472.
- Ohh M, Park CW, Ivan M, Hoffman MA, Kim TY, et al. (2000) Ubiquitination of hypoxia-inducible factor requires direct binding to the beta-domain of the von Hippel-Lindau protein. *Nat Cell Biol* 2: 423–427.
- Shen X, Wan C, Ramaswamy G, Mavalli M, Wang Y, et al. (2009) Prolyl hydroxylase inhibitors increase neoangiogenesis and callus formation following femur fracture in mice. *J Orthop Res* 27: 1298–1305.
- Wang Y, Wan C, Deng L, Liu X, Cao X, et al. (2007) The hypoxia-inducible factor alpha pathway couples angiogenesis to osteogenesis during skeletal development. *J Clin Invest* 117: 1616–1626.

weight of mice in OVX, OVX+L-DMOG and OVX+H-DMOG groups compared to Sham group. (B) OVX significantly decreased the uterus weight. (C) Representative picture of uterus in each group. (D) OVX obviously decreased the BMD of mice. $P < 0.05$ for comparisons among the groups designated with an asterisk. (TIF)

Acknowledgments

This work was supported by the Natural Science Foundation of China (No. 81371958, 81061160510), the Basic Key Project of Science and Technology Commission of Shanghai Municipality (12JC1408200), and the Scientific and Technological Support Program in Biological Medicine of Science and Technology Commission of Shanghai Municipality (13431900702).

Author Contributions

Conceived and designed the experiments: JP ZGL DLF. Performed the experiments: JP ZGL ZLF KH CH SX QJ ZQ WJS QND ZHB. Analyzed the data: JP DLF. Contributed reagents/materials/analysis tools: QND WJS. Contributed to the writing of the manuscript: JP DLF ZGL.

- Rankin EB, Wu C, Khatri R, Wilson TL, Andersen R, et al. (2012) The HIF signaling pathway in osteoblasts directly modulates erythropoiesis through the production of EPO. *Cell* 149: 63–74.
- Weng T, Xie Y, Huang J, Luo F, Yi L, et al. (2014) Inactivation of Vhl in osteochondral progenitor cells causes high bone mass phenotype and protects against age-related bone loss in adult mice. *J Bone Miner Res* 29: 820–829.
- Wan C, Gilbert SR, Wang Y, Cao X, Shen X, et al. (2008) Activation of the hypoxia-inducible factor-1 α pathway accelerates bone regeneration. *Proc Natl Acad Sci U S A* 105: 686–691.
- Wu C, Zhou Y, Chang J, Xiao Y (2013) Delivery of dimethyloxalyl glycine in mesoporous bioactive glass scaffolds to improve angiogenesis and osteogenesis of human bone marrow stromal cells. *Acta Biomater* 9: 9159–9168.
- Fan W, Crawford R, Xiao Y (2010) Enhancing in vivo vascularized bone formation by cobalt chloride-treated bone marrow stromal cells in a tissue engineered periosteum model. *Biomaterials* 31: 3580–3589.
- Wu C, Zhou Y, Fan W, Han P, Chang J, et al. (2012) Hypoxia-mimicking mesoporous bioactive glass scaffolds with controllable cobalt ion release for bone tissue engineering. *Biomaterials* 33: 2076–2085.
- Zou D, Zhang Z, He J, Zhang K, Ye D, et al. (2012) Blood vessel formation in the tissue-engineered bone with the constitutively active form of HIF-1 α mediated BMSCs. *Biomaterials* 33: 2097–2108.
- Zou D, Zhang Z, He J, Zhu S, Wang S, et al. (2011) Repairing critical-sized calvarial defects with BMSCs modified by a constitutively active form of hypoxia-inducible factor-1 α and a phosphate cement scaffold. *Biomaterials* 32: 9707–9718.
- Donneys A, Weiss DM, Deshpande SS, Ahsan S, Tchanque-Fossuo CN, et al. (2013) Localized deferoxamine injection augments vascularity and improves bony union in pathologic fracture healing after radiotherapy. *Bone* 52: 318–325.
- Farberg AS, Jing XL, Monson LA, Donneys A, Tchanque-Fossuo CN, et al. (2012) Deferoxamine reverses radiation induced hypovascularity during bone regeneration and repair in the murine mandible. *Bone* 50: 1184–1187.
- Zhang W, Li G, Deng R, Deng L, Qiu S (2012) New bone formation in a true bone ceramic scaffold loaded with desferrioxamine in the treatment of segmental bone defect: a preliminary study. *J Orthop Sci* 17: 289–298.
- Stewart R, Goldstein J, Eberhardt A, Chu GT, Gilbert S (2011) Increasing vascularity to improve healing of a segmental defect of the rat femur. *J Orthop Trauma* 25: 472–476.
- Ding H, Gao YS, Wang Y, Hu C, Sun Y, et al. (2014) Dimethyloxalylglycine Increases the Bone Healing Capacity of Adipose-Derived Stem Cells by Promoting Osteogenic Differentiation and Angiogenic Potential. *Stem Cells Dev* 23: 990–1000.
- Grewal BS, Keller B, Weinhold P, Dahners LE (2014) Evaluating effects of deferoxamine in a rat tibia critical bone defect model. *J Orthop* 11: 5–9.
- Liu XD, Deng LF, Wang J, Qi J, Zhou Q, et al. (2007) [The regulation of hypoxia inducible factor-1 α on osteoblast function in postmenopausal osteoporosis]. *Zhonghua Wai Ke Za Zhi* 45: 1274–1278.
- Zhao Q, Shen X, Zhang W, Zhu G, Qi J, et al. (2012) Mice with increased angiogenesis and osteogenesis due to conditional activation of HIF pathway in osteoblasts are protected from ovariectomy induced bone loss. *Bone* 50: 763–770.
- Yun SP, Lee MY, Ryu JM, Song CH, Han HJ (2009) Role of HIF-1 α and VEGF in human mesenchymal stem cell proliferation by 17 β -estradiol: involvement of PKC, PI3K/Akt, and MAPKs. *Am J Physiol Cell Physiol* 296: C317–326.

35. Yen ML, Su JL, Chien CL, Tseng KW, Yang CY, et al. (2005) Diosgenin induces hypoxia-inducible factor-1 activation and angiogenesis through estrogen receptor-related phosphatidylinositol 3-kinase/Akt and p38 mitogen-activated protein kinase pathways in osteoblasts. *Mol Pharmacol* 68: 1061–1073.
36. Mazumdar J, O'Brien WT, Johnson RS, LaManna JC, Chavez JC, et al. (2010) O₂ regulates stem cells through Wnt/beta-catenin signalling. *Nat Cell Biol* 12: 1007–1013.
37. Ren H, Cao Y, Zhao Q, Li J, Zhou C, et al. (2006) Proliferation and differentiation of bone marrow stromal cells under hypoxic conditions. *Biochem Biophys Res Commun* 347: 12–21.
38. Wagegg M, Gaber T, Lohanatha FL, Hahne M, Strehl C, et al. (2012) Hypoxia promotes osteogenesis but suppresses adipogenesis of human mesenchymal stromal cells in a hypoxia-inducible factor-1 dependent manner. *PLoS One* 7: e46483.
39. Zou D, Zhang Z, Ye D, Tang A, Deng L, et al. (2011) Repair of critical-sized rat calvarial defects using genetically engineered bone marrow-derived mesenchymal stem cells overexpressing hypoxia-inducible factor-1alpha. *Stem Cells* 29: 1380–1390.
40. Qu Z-H, Zhang X-L, Tang T-T, Dai K-R (2008) Promotion of osteogenesis through beta-catenin signaling by desferrioxamine. *Biochem Biophys Res Commun* 370: 332–337.
41. Genetos DC, Toupadakis CA, Raheja LF, Wong A, Papanicolaou SE, et al. (2010) Hypoxia decreases sclerostin expression and increases Wnt signaling in osteoblasts. *J Cell Biochem* 110: 457–467.
42. Bidwell JP, Alvarez MB, Hood M Jr, Childress P (2013) Functional impairment of bone formation in the pathogenesis of osteoporosis: the bone marrow regenerative competence. *Curr Osteoporos Rep* 11: 117–125.
43. Li L, Yao XL, He XL, Liu XJ, Wu WC, et al. (2013) Role of mechanical strain and estrogen in modulating osteogenic differentiation of mesenchymal stem cells (MSCs) from normal and ovariectomized rats. *Cell Mol Biol (Noisy-le-grand) Suppl* 59: OL1889–1893.
44. Yang N, Wang G, Hu C, Shi Y, Liao L, et al. (2013) Tumor necrosis factor alpha suppresses the mesenchymal stem cell osteogenesis promoter miR-21 in estrogen deficiency-induced osteoporosis. *J Bone Miner Res* 28: 559–573.
45. Kusumbe AP, Ramasamy SK, Adams RH (2014) Coupling of angiogenesis and osteogenesis by a specific vessel subtype in bone. *Nature* 507: 323–328.
46. Jia P, Xu YJ, Zhang ZL, Li K, Li B, et al. (2012) Ferric ion could facilitate osteoclast differentiation and bone resorption through the production of reactive oxygen species. *J Orthop Res* 30: 1843–1852.
47. Ishii KA, Fumoto T, Iwai K, Takeshita S, Ito M, et al. (2009) Coordination of PGC-1beta and iron uptake in mitochondrial biogenesis and osteoclast activation. *Nat Med* 15: 259–266.
48. Zhao HX, Wang XL, Wang YH, Wu Y, Li XY, et al. (2010) Attenuation of myocardial injury by postconditioning: role of hypoxia inducible factor-1alpha. *Basic Res Cardiol* 105: 109–118.
49. Song YR, You SJ, Lee YM, Chin HJ, Chae DW, et al. (2010) Activation of hypoxia-inducible factor attenuates renal injury in rat remnant kidney. *Nephrol Dial Transplant* 25: 77–85.
50. Takaku M, Tomita S, Kurobe H, Kihira Y, Morimoto A, et al. (2012) Systemic preconditioning by a prolyl hydroxylase inhibitor promotes prevention of skin flap necrosis via HIF-1-induced bone marrow-derived cells. *PLoS One* 7: e42964.
51. Botusan IR, Sunkari VG, Savu O, Catrina AI, Grunler J, et al. (2008) Stabilization of HIF-1alpha is critical to improve wound healing in diabetic mice. *Proc Natl Acad Sci U S A* 105: 19426–19431.
52. Rey S, Lee K, Wang CJ, Gupta K, Chen S, et al. (2009) Synergistic effect of HIF-1alpha gene therapy and HIF-1-activated bone marrow-derived angiogenic cells in a mouse model of limb ischemia. *Proc Natl Acad Sci U S A* 106: 20399–20404.
53. Poynter JA, Manukyan MC, Wang Y, Brewster BD, Herrmann JL, et al. (2011) Systemic pretreatment with dimethylallylglycine increases myocardial HIF-1alpha and VEGF production and improves functional recovery after acute ischemia/reperfusion. *Surgery* 150: 278–283.
54. Patel TH, Kimura H, Weiss CR, Semenza GL, Hofmann LV (2005) Constitutively active HIF-1alpha improves perfusion and arterial remodeling in an endovascular model of limb ischemia. *Cardiovasc Res* 68: 144–154.
55. Sun Y, Li QF, Zhang Y, Hu R, Jiang H (2013) Isoflurane preconditioning increases survival of rat skin random-pattern flaps by induction of HIF-1alpha expression. *Cell Physiol Biochem* 31: 579–591.
56. Dempster DW, Compston JE, Drezner MK, Glorieux FH, Kanis JA, et al. (2013) Standardized nomenclature, symbols, and units for bone histomorphometry: a 2012 update of the report of the ASBMR Histomorphometry Nomenclature Committee. *J Bone Miner Res* 28: 2–17.
57. Zelzer E, Levy Y, Kahana C, Shilo BZ, Rubinstein M, et al. (1998) Insulin induces transcription of target genes through the hypoxia-inducible factor HIF-1alpha/ARNT. *EMBO J* 17: 5085–5094.
58. Fukuda R, Hirota K, Fan F, Jung YD, Ellis LM, et al. (2002) Insulin-like growth factor 1 induces hypoxia-inducible factor 1-mediated vascular endothelial growth factor expression, which is dependent on MAP kinase and phosphatidylinositol 3-kinase signaling in colon cancer cells. *J Biol Chem* 277: 38205–38211.
59. Botusan IR, Sunkari VG, Savu O, Catrina AI, Grunler J, et al. (2008) Stabilization of HIF-1 is critical to improve wound healing in diabetic mice. *Proceedings of the National Academy of Sciences* 105: 19426–19431.
60. Long F (2012) Building strong bones: molecular regulation of the osteoblast lineage. *Nat Rev Mol Cell Biol* 13: 27–38.
61. Rossini M, Gatti D, Adami S (2013) Involvement of WNT/beta-catenin signaling in the treatment of osteoporosis. *Calcif Tissue Int* 93: 121–132.
62. Xu XJ, Shen L, Yang YP, Zhu R, Shuai B, et al. (2013) Serum beta -Catenin Levels Associated with the Ratio of RANKL/OPG in Patients with Postmenopausal Osteoporosis. *Int J Endocrinol* 2013: 534352.
63. Shin DH, Kim JH, Jung YJ, Kim KE, Jeong JM, et al. (2007) Preclinical evaluation of YC-1, a HIF inhibitor, for the prevention of tumor spreading. *Cancer Lett* 255: 107–116.
64. Liu L, Yu Q, Lin J, Lai X, Cao W, et al. (2011) Hypoxia-inducible factor-1alpha is essential for hypoxia-induced mesenchymal stem cell mobilization into the peripheral blood. *Stem Cells Dev* 20: 1961–1971.
65. van de Wetering M, Cavallo R, Dooijes D, van Beest M, van Es J, et al. (1997) Armadillo coactivates transcription driven by the product of the *Drosophila* segment polarity gene dTCF. *Cell* 88: 789–799.
66. Reya T, Clevers H (2005) Wnt signalling in stem cells and cancer. *Nature* 434: 843–850.
67. Bouxsein ML, Boyd SK, Christiansen BA, Guldberg RE, Jepsen KJ, et al. (2010) Guidelines for assessment of bone microstructure in rodents using micro-computed tomography. *J Bone Miner Res* 25: 1468–1486.
68. Liu Y, Berendsen AD, Jia S, Lotinun S, Baron R, et al. (2012) Intracellular VEGF regulates the balance between osteoblast and adipocyte differentiation. *J Clin Invest* 122: 3101–3113.
69. Chapurlat RD, Delmas PD (2009) Bone microdamage: a clinical perspective. *Osteoporos Int* 20: 1299–1308.
70. Maes C, Goossens S, Bartunkova S, Drogat B, Coenegrachts L, et al. (2010) Increased skeletal VEGF enhances beta-catenin activity and results in excessively ossified bones. *EMBO J* 29: 424–441.
71. Henriksen K, Tanko LB, Qvist P, Delmas PD, Christiansen C, et al. (2007) Assessment of osteoclast number and function: application in the development of new and improved treatment modalities for bone diseases. *Osteoporos Int* 18: 681–685.
72. Spencer GJ, Utting JC, Etheridge SL, Arnett TR, Genever PG (2006) Wnt signalling in osteoblasts regulates expression of the receptor activator of NFkappaB ligand and inhibits osteoclastogenesis in vitro. *J Cell Sci* 119: 1283–1296.